Structural Basis for Catalytic Differences between α Class Human Glutathione Transferases hGSTA1-1 and hGSTA2-2 for Glutathione Conjugation of Environmental Carcinogen Benzo[*a*]pyrene-7,8-diol-9,10-epoxide†

Shivendra V. Singh,*,‡ Vijayalakshmi Varma,§ Piotr Zimniak,§ Sanjay K. Srivastava,‡ Stanley W. Marynowski,‡ Dhimant Desai,|| Shantu Amin,|| and Xinhua Ji⊥

Department of Pharmacology and University of Pittsburgh Cancer Institute, University of Pittsburgh School of Medicine, Pittsburgh, Pennsylvania 15213, Department of Pharmacology and Toxicology, University of Arkansas for Medical Sciences, and Central Arkansas Veterans Healthcare System, Little Rock, Arkansas 72205, Institute for Cancer Prevention, Valhalla, New York 10595, and Macromolecular Crystallography Laboratory, National Cancer Institute, Frederick, Maryland 21702

Received March 23, 2004; Revised Manuscript Received May 25, 2004

ABSTRACT: The ultimate diol epoxide carcinogens derived from polycyclic aromatic hydrocarbons, such as benzo[*a*]pyrene (BP), are metabolized primarily by glutathione (GSH) conjugation reaction catalyzed by GSH transferases (GSTs). In human liver and probably lung, the α class GSTs are likely to be responsible for the majority of this reaction because of their high abundance. The catalytic efficiency for GSH conjugation of the carcinogenic (+)-*anti*-benzo[*a*]pyrene-7,8-diol-9,10-epoxide [(+)-*anti*-BPDE] is more than 5-fold higher for hGSTA1-1 than for hGSTA2-2. Here, we demonstrate that mutation of isoleucine-11 of hGSTA2-2, a residue located in the hydrophobic substrate-binding site (H-site) of the enzyme, to alanine (which is present in the same position in hGSTA1-1) results in about a 7-fold increase in catalytic efficiency for (+)-*anti*-BPDE−GSH conjugation. Thus, a single amino acid substitution is sufficient to convert hGSTA2-2 to a protein that matches hGSTA1-1 in its catalytic efficiency. The increased catalytic efficiency of hGSTA2/I11A is accompanied by greater enantioselectivity for the carcinogenic (+)-*anti*-BPDE over (−)-*anti*-BPDE. Further remodeling of the H-site of hGSTA2-2 to resemble that of hGSTA1-1 (S9F, I11A, F110V, and S215A mutations, SIFS mutant) results in an enzyme whose catalytic efficiency is approximately 13.5-fold higher than that of the wild-type hGSTA2-2, and about 2.5-fold higher than that of the wild-type hGSTA1-1. The increased activity upon mutations can be rationalized by the interactions of the amino acid side chains with the substrate and the orientation of the substrate in the active site, as visualized by molecular modeling. Interestingly, the catalytic efficiency of hGSTA2-2 toward (−)-*anti*-BPDE was increased to a level close to that of hGSTA1-1 upon F110V, not I11A, mutation. Similar to (+)-*anti*-BPDE, however, the SIFS mutant was the most efficient enzyme for GSH conjugation of (−)-*anti*-BPDE.

Benzo[*a*]pyrene (BP)[1] is the prototype and best characterized member of the polycyclic aromatic hydrocarbon (PAH) family of environmental pollutants that are abundant in cigarette smoke, automobile exhaust, barbecued food, and so forth (*1*). PAHs are tumorigenic in experimental animals and suspected human carcinogens (*1*−*3*). The tumorigenic activity of BP is mainly attributed to its diol epoxide isomer (7*R*,8*S*)-dihydroxy-(9*S*,10*R*)-epoxy-7,8,9,10-tetrahydrobenzo-[*a*]pyrene [(+)-*anti*-BPDE] (refer to Figure 1 for the structure and absolute configuration of *anti*-BPDE isomers) (*2*, *3*), which is highly reactive toward nucleophilic sites in DNA (*4*−*6*). Several different mechanisms have been identified that can offer protection against covalent interaction of (+)-*anti*-BPDE with nucleophilic sites in DNA, including spontaneous hydrolysis, hydration by epoxide hydrolase, and glutathione (GSH) transferase (GST)-catalyzed conjugation with GSH (*7*−*12*). Furthermore, riboflavin 5′-phosphate, ellagic acid (a plant phenol), and certain phenolic metabolites of BP have been shown to inhibit mutagenic and/or tumorigenic activity of *anti*-BPDE (*13*−*16*). However, the GST-catalyzed GSH conjugation of (+)-*anti*-BPDE is believed to be the most important enzymatic mechanism for its inactivation (*10*−*12*). The importance of GSTs in protection against (+)-*anti*-BPDE is supported by the following ob-

† This work was supported in part by U.S. Public Health Service Grant CA076348 (to S.V.S.), awarded by the National Cancer Institute, and Grant ES09140 (to S.V.S. and P.Z.), awarded by the National Institute of Environmental Health Sciences.

* To whom correspondence should be addressed. Phone: (412) 623-3263. Fax: (412) 623-7828. E-mail: singhs@upmc.edu.

‡ University of Pittsburgh School of Medicine.

§ University of Arkansas for Medical Sciences and Central Arkansas Veterans Healthcare System.

|| Institute for Cancer Prevention.

⊥ National Cancer Institute.

[1] Abbreviations: BP, benzo[*a*]pyrene; (±)-*anti*-BPDE, racemic *anti*-7,8-dihydroxy-9,10-epoxy-7,8,9,10-tetrahydrobenzo[*a*]pyrene; CDNB, 1-chloro-2,4-dinitrobenzene; GSH, glutathione; GSBpd, GSH conjugate of (+)-*anti*-BPDE; GSEa, GSH conjugate of ethacrynic acid; hGSTA1-1, α class human GSH transferase A1-1; hGSTA2-2, α class human GSH transferase A2-2; mGSTA1-1, murine α class GSH transferase A1-1; PAH, polycyclic aromatic hydrocarbon; TKE buffer, 50 mM Tris−HCl (pH 7.5) containing 2.5 mM KCl and 0.5 mM EDTA.

10.1021/bi049435f CCC: $27.50
Published on Web 07/10/2004

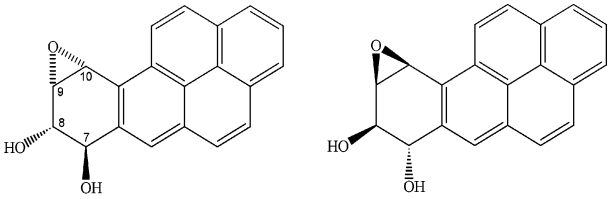

(+)-(7*R*,8*S*,9*S*,10*R*)-BPDE (-)-(7*S*,8*R*,9*R*,10*S*)-BPDE

FIGURE 1: Structure and absolute configuration of (+)- and (−)-enantiomers of *anti*- BPDE.

servations: (a) the GSH conjugation of (+)-*anti*-BPDE is significantly increased in the presence of purified GST isozymes (*10*−*12*), (b) ectopic expression of GSTs offers significant protection against interaction of *anti*-BPDE with DNA (*17*−*19*), and (c), D,L-buthionine-(*S*,*R*)-sulfoximine-mediated depletion of tissue GSH levels, which is likely to compromise GSH conjugation of (+)-*anti*-BPDE, increases sensitivity of mice to BP-induced tumorigenesis (*20*).

GSTs are a superfamily of multifunctional isozymes that can detoxify a wide variety of electrophilic xenobiotics primarily by catalyzing their conjugation with GSH (*21*, *22*). Cytosolic GST activity is due to multiple isozymes, which have been grouped into several classes, namely, α, μ, π (*23*), θ (*24*), σ (*25*), κ (*26*), and ζ (*27*). At least four α class GST gene products (hGSTA1-1, hGSTA2-2, hGSTA3-3, and hGSTA4-4) are expressed in human tissues (*28*−*31*), which differ remarkably in their substrate specificity (*30*, *32*, *33*). For example, both hGSTA1-1 and hGSTA2-2 exhibit high selenium-independent GSH peroxidase activity toward fatty acid hydroperoxides and phospholipid hydroperoxides (*33*), whereas hGSTA3-3 is a highly efficient catalyst of double-bond isomerization of intermediates in steroid hormone biosynthesis, e.g., Δ^5-androstene-3,17-dione (*30*). The GSH conjugation of alkenals is preferentially catalyzed by the hGSTA4-4 isoform (*31*, *32*). Distribution of α class GSTs is highly variable in human tissues. For instance, hGSTA1-1 and hGSTA2-2 isoforms are the predominant α class GSTs in human liver (the major site for xenobiotic biotransformation) and lung (a target organ for PAH-induced cancer) (*34*, *35*), whereas the message for hGSTA3 is not detectable in human liver (*30*).

hGSTA1-1 and hGSTA2-2 are structurally closely related with about 95% amino acid identity, yet the two isoforms differ significantly in their activity toward (+)-*anti*-BPDE (*36*). The crystal structure of hGSTA1-1 has provided insights into the amino acid residues that constitute the hydrophobic-substrate-binding site (H-site) and the GSH-binding site (G-site) (*37*). The amino acid sequences of hGSTA1-1 and hGSTA2-2 differ at 10 positions (*28*, *29*). While the G-site-defining residues are conserved between hGSTA1-1 and hGSTA2-2, the H-site-defining residues between these isoforms differ at four positions (positions 9, 11, 110, and 215). Here, we provide experimental evidence to indicate that the catalytic difference between hGSTA1-1 and hGSTA2-2 toward (+)-*anti*-BPDE is solely attributable to the amino acid substitution in position 11 (alanine in hGSTA1-1 and isoleucine in hGSTA2-2).

MATERIALS AND METHODS

Site-Directed Mutagenesis. The bacterial expression vectors pET30a/hGSTA1 and pET30a/hGSTA2 were generous gifts from Prof. Y. C. Awasthi (University of Texas Medical Branch, Galveston, TX) (*33*). Single mutants of hGSTA2-2 encoding S9F, I11A, F110V, and S215A were obtained using the QuickChange Site-Directed Mutagenesis Kit (Stratagene) with the sense primers 5′-CC AAG CTC CAC TAC T*T*C AAT ATA CG**T** GGC AG, 5′-CAC TAC TCC AAT *GC*A CG**T** GGC AGA ATG, 5′-TC CTT CTT CTG CCC *G*TT ACT CAA CCT GAG, and 5′-G GAT GAG AAA TCT TTA GAA GAA *G*CA AGG AAG ATT TTC AGG, respectively, together with the corresponding antisense primers (mutation sites are italic). Primers used to introduce the S9F and I11A mutations also introduced a silent mutation of A12 (CGG to CGT) to prevent a run of four G's, which presents problems in oligonucleotide synthesis (the changed nucleotides are shown in bold). To obtain the quadruple mutant S9F + I11A + F110V +S215A, the S9F + I11A mutation was introduced (sense primer 5′-CCC AAG CTC CAC TAC T*T*C AAT *GC*A CG**T** GGC AGA ATG GAG TCC ATC) to the plasmid pET30a/hGSTA2(F110V + S215A) that was obtained first by the QuickChange Multi Site-Directed Mutagenesis Kit (Stratagene) with two sense primers (5′-/5Phos/TC CTT CTT CTG CCC *G*TT ACT CAA CCT GAG and 5′-/5Phos/G GAT GAG AAA TCT TTA GAA GAA *G*CA AGG AAG ATT TTC AGG). All mutations were confirmed by sequencing of the entire open reading frame of hGSTA2. The *E. coli* expression host BL-21 Star(DE3)-pLysS (Invitrogen) was transformed with wild-type hGSTA1 or hGSTA2 as well as the mutant hGSTA2 plasmids, and cultured in the presence of 50 μg/mL kanamycin and 34 μg/mL chloramphenicol at 37 °C. At a cell density of A_{600} = 0.6, IPTG was added to a final concentration of 0.5 mM, and the cells were collected 5 h later.

GST Purification. A bacterial pellet was suspended in 22 mM potassium phosphate buffer, pH 7.0, containing 1.4 mM 2-mercaptoethanol (affinity buffer), sonicated, and centrifuged at 14000*g* for 45 min. The supernatant fraction was dialyzed overnight against affinity buffer and subjected to GSH affinity chromatography according to the method of Simons and Vander Jagt (*38*) with some modifications described by us previously (*39*). The GST was eluted with 10 mM GSH in 50 mM Tris−HCl (pH 9.5) containing 1.4 mM 2-mercaptoethanol. Purification of the GST protein was monitored by determining the enzyme activity toward 1-chloro-2,4-dinitrobenzene (CDNB) as described by Habig et al. (*40*). The protein content was measured by Bradford's method (*41*). The purity of each GST preparation was ascertained by sodium dodecyl sulfate−polyacrylamide gel electrophoresis (*42*) prior to the kinetic studies. A single protein band was observed for each preparation.

GST Activity Determination. The GST activity toward *anti*-BPDE was determined as described by us previously (*43*, *44*). Briefly, the reaction mixture in a final volume of 0.1 mL contained 50 mM Tris−HCl, pH 7.5, containing 2.5 mM KCl and 0.5 mM EDTA (TKE buffer), 2 mM GSH, 20 μg/mL (wild-type hGSTA1-1) or 40 μg/mL (wild-type hGSTA2-2 and mutants of hGSTA2-2) GST protein, and the desired concentration of (±)-*anti*-BPDE. The reaction was initiated by adding (±)-*anti*-BPDE, and the reaction mixture was incubated for 30 s at 37 °C. The reaction was stopped by rapid mixing with 0.1 mL of cold acetone, followed by extraction with ethyl acetate saturated with TKE buffer. The GSH conjugates of (+)- and (−)-*anti*-BPDE in the aqueous

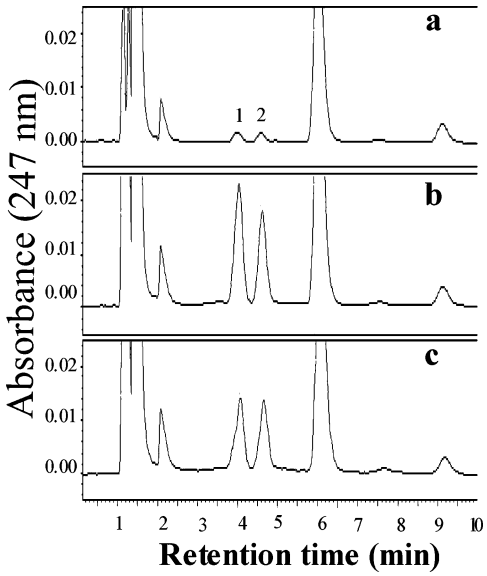

FIGURE 2: Reversed-phase HPLC elution profile for water-soluble products resulting from the reaction of 2 mM GSH and 120 μM (±)-*anti*-BPDE in the absence of GST protein (panel a) and in the presence of 20 μg/mL hGSTA1-1 (panel b) and 40 μg/mL hGSTA2-2 (panel c). The GSH conjugates of (+)-*anti*- and (−)-*anti*-BPDE eluted at retention times of 4.0 and 4.6 min, respectively (denoted by the numbers 1 and 2, respectively, in panel a). The identity of the GSH conjugates was ascertained by reversed-phase HPLC analysis of authentic standards.

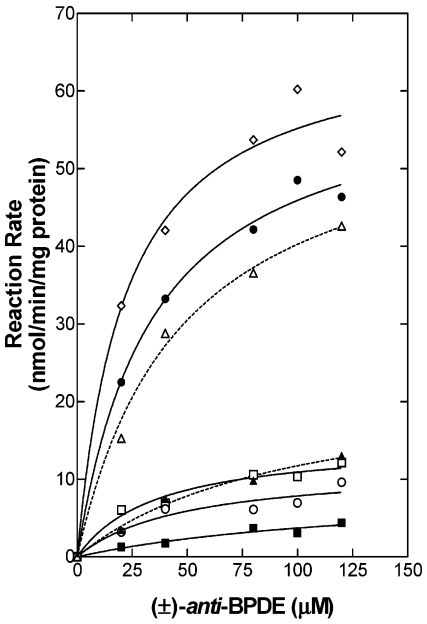

FIGURE 3: Rate of GSH conjugation of (+)-*anti*-BPDE as a function of varying diol epoxide concentration (10−120 μM) in the presence of 20 μg/mL wild-type hGSTA1-1 (empty triangle, dotted line), 40 μg/mL wild-type hGSTA2-2 (filled triangle, dotted line), 40 μg/mL hGSTA2/S9F mutant (empty circle, solid line), 40 μg/mL hGSTA2/I11A mutant (filled circle, solid line), 40 μg/mL hGSTA2/F110V mutant (empty square, solid line), 40 μg/mL hGSTA2/S215A mutant (filled square, solid line), and 40 μg/mL hGSTA2/SIFS mutant (empty tilted square, solid line).

phase were resolved and quantified by reversed-phase HPLC as described by us previously (*43*, *44*). A blank was included to account for nonenzymatic GSH conjugation of *anti*-BPDE enantiomers. The GST activity was determined as a function of varying (±)-*anti*-BPDE concentrations (10−120 μM) at a fixed saturating concentration of GSH (2 mM) to determine the kinetic constants. For determination of the kinetic constant toward CDNB, the GST activity was determined as a function of varying CDNB concentrations (0.1−1.2 mM) at a fixed 1 mM GSH concentration at 25 °C essentially as described by Habig et al. (*40*).

RESULTS AND DISCUSSION

Enantioselectivity and Catalytic Efficiency of hGSTA1-1 and hGSTA2-2 toward anti-BPDE. Figure 2 depicts the reversed-phase HPLC elution profiles of water-soluble products resulting from the reaction of 2 mM GSH and 120 μM (±)-*anti*-BPDE in the absence of GST protein (panel a) and in the presence of wild-type hGSTA1-1 (panel b) and wild-type hGSTA2-2 (panel c). The GSH conjugates of (+)-*anti*-BPDE and (−)-*anti*-BPDE, which were identified by reversed-phase HPLC analysis of authentic standards, eluted at retention times of about 4.0 and 4.6 min, respectively (Figure 2a). Other peaks in the HPLC tracings were identified by analysis of the components of the reaction mixture individually [e.g., TKE buffer alone, GSH alone, or (±)-*anti*-BPDE alone] or in combination [e.g., TKE buffer + GSH, TKE buffer + (±)-*anti*-BPDE, or TKE buffer + GSH + (±)-*anti*-BPDE]. The peak eluting at a retention time of about 1.5 min was GSH, whereas the peak at 2.5 min was an impurity of the GSH preparation (perhaps oxidized glutathione). The *anti*-BPDE is highly unstable in aqueous solutions and rapidly converted to benzo[*a*]pyrene-7,8,9,10-tetrol (*5*), which eluted at a retention time of about 6.2 min. The identity of the peak eluting at a retention time of about 9.2 min, which was observed only if (±)-*anti*-BPDE was present in the reaction mixture, could not be established. As can be seen in Figure 2a, the GSH conjugation of (+)-*anti*-BPDE was very low in the absence of GST protein, and was increased by about 15- and 10-fold in the presence of hGSTA1-1 (Figure 2b) and hGSTA2-2 (Figure 2c), respectively. Similarly, the GSH conjugation of (−)-*anti*-BPDE (denoted by the number 2 in Figure 2a) was increased significantly in the presence of both isoforms. Moreover, while hGSTA1-1 exhibited slight preference toward GSH conjugation of the (+)-*anti*-isomer [about 57% vs 43% for (−)-*anti*-BPDE) (Figure 2b), hGSTA2-2 was equally effective in catalyzing the GSH conjugation of both isomers [51% and 49% for (+)-*anti*-BPDE and (−)-*anti*-BPDE, respectively, Figure 2c).

Activities of hGSTA1-1 and hGSTA2-2 were determined as a function of varying diol epoxide concentration (10−120 μM) at a fixed saturating concentration of GSH (2 mM) to determine the kinetic constants. As shown in Figure 3, both hGSTA1-1 and hGSTA2-2 followed Michaelis−Menten kinetics when GST activity was measured as a function of varying (±)-*anti*-BPDE concentrations. The kinetic constants for wild-type hGSTA1-1 and hGSTA2-2 toward (+)-*anti*-BPDE are summarized in Table 1. The catalytic efficiency of hGSTA1-1 (1.1 mM^{-1} s^{-1}) was >5-fold higher compared with that of hGSTA2-2, which was attributable to an approximately 2.6-fold higher V_{max} and about 50% lower K_m value for the former isoform than those for hGSTA2-2 (Table 1).

Effects of Mutations of Variant H-Site Residues on the Activity of hGSTA2-2 toward (+)-anti-BPDE. On the basis of the three-dimensional structure of the protein, the GSH-

Table 1: Kinetic Constants for Wild-Type hGSTA1-1 and hGSTA2-2 and Mutants of hGSTA2-2 toward (+)-*anti*-BPDE[a]

isozyme	V_{max} [(nmol/min)/mg]	K_m (μM)	k_{cat} (s^{-1})	k_{cat}/K_m ($mM^{-1}\,s^{-1}$)
		Wild-Type Isozymes		
hGSTA1-1	59 ± 8*	47 ± 16	0.05 ± 0.007*	1.1 ± 0.22**
hGSTA2-2	23 ± 4*	98 ± 30	0.02 ± 0.003*	0.2 ± 0.03**
		Mutants of hGSTA2-2		
hGSTA2/S9F	12 ± 2*	49 ± 22	0.01 ± 0.002*	0.2 ± 0.06
hGSTA2/I11A	62 ± 4**	35 ± 6	0.05 ± 0.003**	1.4 ± 0.2**
hGSTA2/F110V	15 ± 1*	36 ± 10	0.012 ± 0.001*	0.3 ± 0.06**
hGSTA2/S215A	9 ± 4**	143 ± 114	0.008 ± 0.003**	0.06 ± 0.02**
hGSTA2/SIFS[b]	67 ± 5**	22 ± 6	0.06 ± 0.004**	2.7 ± 0.5**

[a] Wild-type hGSTA1-1 (20 μg/mL), wild-type hGSTA2-2 (40 μg/mL), and each mutant of hGSTA2-2 (40 μg/mL) were incubated with 10−120 μM (±)-*anti*-BPDE and 2 mM GSH in 50 mM Tris−HCl (pH 7.5) containing 2.5 mM KCl and 0.5 mM EDTA (TKE buffer) for 30 s at 37 °C. The GSH conjugate of (+)-*anti*-BPDE was resolved and quantified by reversed-phase HPLC as described by us previously (*43*, *44*). Kinetic parameters were estimated by fitting a hyperbolic function to the experimental data points through nonlinear regression analysis, and are shown ± asymptotic standard error. For the wild-type isozymes, a single asterisk denotes that the parameter is different between hGSTA1-1 and hGSTA2-2 at $p = 0.02$; a double asterisk denotes $p = 0.001$. The statistical significance between a given mutant and wild-type hGSTA2-2 is denoted as follows: $*p < 0.1$; $**p \leq 0.05$. Kinetic determinations were performed in triplicate, and the experiment was repeated to ensure reproducibility. [b] The hGSTA2-2 mutant with combined mutations of S9F, I11A, F110V, and S215A.

Table 2: Differences in Amino Acid Sequences between hGSTA1-1 and hGSTA2-2

position[a]	hGSTA1-1	hGSTA2-2	H-site
9	phenylalanine	serine	yes
11	alanine	isoleucine	yes
18	threonine	isoleucine	no
88	arginine	lysine	no
110	valine	phenylalanine	yes
111	cysteine	threonine	no
113	proline	glutamine	no
116	lysine	glutamine	no
124	lysine	glutamine	no
215	alanine	serine	yes

[a] Excluding initiator methionine.

binding-site (G-site) residues in hGSTA1-1 include Y8, R14, R44, Q53, V54, Q66, T67, D100, R130, and F219 (numbering excludes initiator methionine). The amino acid residues assigned to the hydrophobic-substrate-binding site (H-site) of hGSTA1-1 are F9, A11, G13, E103, L106, L107, P109, V110, M207, L212, A215, and F221 (*37*). The amino acid sequence alignment of hGSTA1-1 and hGSTA2-2 reveals 10 substitutions (summarized in Table 2), but only 4 of these changes are located in the H-site (Table 2). On the other hand, the G-site-defining residues are conserved between hGSTA1-1 and hGSTA2-2. We hypothesized that the H-site amino acid substitution(s) might contribute to catalytic differences between hGSTA1-1 and hGSTA2-2 toward (+)-*anti*-BPDE. We experimentally tested the above hypothesis by determining the (+)-*anti*-BPDE−GSH conjugating activities of the mutants of hGSTA2-2 in which amino acid residues in positions 9, 11, 110, and 215 were mutated to the corresponding residues of hGSTA1-1 (hereafter designated as hGSTA2/S9F, hGSTA2/I11A, hGSTA2/F110V, and hGSTA2/S215A).

As shown in Figure 3, similar to the wild-type hGSTA1-1 and hGSTA2-2, each mutant of hGSTA2-2 adhered to the Michaelis−Menten kinetics. The kinetic constants for the mutants of hGSTA2-2 toward (+)-*anti*-BPDE are also summarized in Table 1. The catalytic efficiency of hGSTA2-2 for GSH conjugation of (+)-*anti*-BPDE was not affected by S9F mutation, although the V_{max} and the K_m values of the hGSTA2/S9F mutant were approximately 50% lower compared with those of the wild-type hGSTA2-2

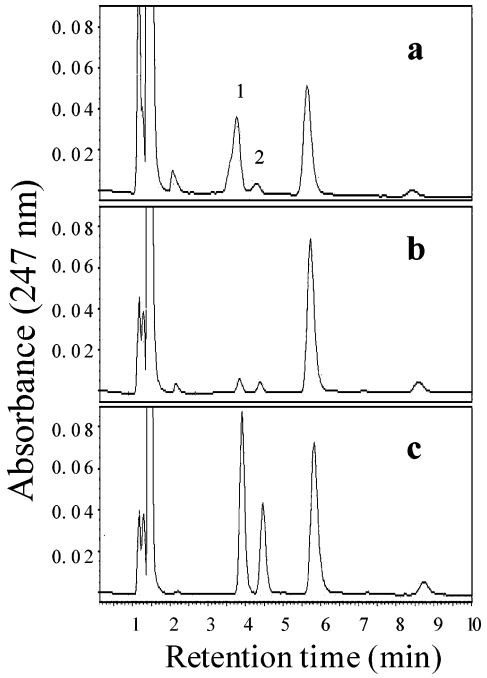

FIGURE 4: Reversed-phase HPLC elution profile for water-soluble products resulting from the reaction of 2 mM GSH and 120 μM (±)-*anti*-BPDE in the presence of 40 μg/mL hGSTA2/I11A (panel a), hGSTA2/F110V (panel b), and hGSTA2/SIFS (panel c). In panel a, the GSH conjugates of (+)-*anti*-BPDE and (−)-*anti*-BPDE are respectively identified by the numbers 1 and 2.

(Table 1). The I11A mutation resulted in a pronounced increase in catalytic efficiency of hGSTA2-2 toward (+)-*anti*-BPDE. In fact, the catalytic efficiency of the hGSTA2/I11A mutant was similar to that of the wild-type hGSTA1-1 (Table 1). This was due to a 2.7-fold increase in the V_{max} and about 64% reduction in the K_m of the mutant protein compared with the wild-type hGSTA2-2. The reversed-phase HPLC elution profile for GSH conjugates of *anti*-BPDE enantiomers in the presence of hGSTA2/I11A mutant protein (40 μg/mL) is shown in Figure 4a. It is interesting to note that the hGSTA2/I11A mutant exhibited an almost exclusive preference toward (+)-*anti*-BPDE, with about 85% of the GSH conjugation occurring with this enantiomer (Figure 4a, denoted as peak 1). The V_{max} and the K_m values for the F110V mutant were lower by about 35% and 63%, respec-

Table 3: Kinetic Constants for Wild-Type hGSTA1-1 and hGSTA2-2 and Mutants of hGSTA2-2 toward (−)-*anti*-BPDE[a]

isozyme	V_{max} [(nmol/min)/mg]	K_m (μM)	k_{cat} (s^{-1})	k_{cat}/K_m ($mM^{-1}\,s^{-1}$)
		Wild-Type Isozymes		
hGSTA1-1	23 ± 3	46 ± 17	0.019 ± 0.002	0.41 ± 0.1
hGSTA2-2	26 ± 5	123 ± 39	0.021 ± 0.004	0.18 ± 0.02
		Mutants of hGSTA2-2		
hGSTA2/S9F	7 ± 1**	43 ± 18*	0.006 ± 0.001**	0.13 ± 0.04
hGSTA2/I11A	11 ± 3**	96 ± 44	0.009 ± 0.002**	0.09 ± 0.02**
hGSTA2/F110V	14 ± 2*	36 ± 12	0.011 ± 0.001*	0.30 ± 0.07*
hGSTA2/S215A	10 ± 6*	214 ± 201	0.008 ± 0.005*	0.04 ± 0.01**
hGSTA2/SIFS[b]	33 ± 3	11 ± 5	0.027 ± 0.002	2.50 ± 0.98**

[a] Wild-type and mutant enzymes were incubated with 10−120 μM (±)-*anti*-BPDE and 2 mM GSH in TKE buffer for 30 s at 37 °C. The GSH conjugate of (−)-*anti*-BPDE was resolved and quantified by reversed-phase HPLC as described by us previously (*43*, *44*). Kinetic parameters were estimated by fitting a hyperbolic function to the experimental data points through nonlinear regression analysis, and are shown ± asymptotic standard error. The catalytic efficiency of the wild-type hGSTA2-2 was significantly different from that of the wild-type hGSTA1-1 ($p = 0.02$), while the null hypothesis could not be rejected for V_{max} and K_m ($p > 0.02$). The statistical significance between a given mutant and wild-type hGSTA2-2 is denoted as follows: *$p < 0.1$; **$p \leq 0.03$. Kinetic determinations were performed in triplicate, and the experiment was repeated to ensure reproducibility. [b] hGSTA2-2 variant with combined mutations of S9F, I11A, F110V, and S215A.

Table 4: Kinetic Constants for Wild-Type hGSTA1-1 and hGSTA2-2 and Mutants of hGSTA2-2 toward CDNB[a]

isozyme	V_{max} [(μmol/min)/mg]	K_m (mM)	k_{cat} (s^{-1})	k_{cat}/K_m ($mM^{-1}\,s^{-1}$)
		Wild-Type Isozymes		
hGSTA1-1	56 ± 4	0.3 ± 0.07	46 ± 3	153 ± 18
hGSTA2-2	18 ± 2	0.5 ± 0.13	15 ± 2	30 ± 6
		Mutants of hGSTA2-2		
hGSTA2/S9F	53 ± 13**	1.6 ± 0.59*	44 ± 11**	28 ± 4
hGSTA2/I11A	3 ± 0.2**	0.06 ± 0.02**	2.6 ± 0.1**	43 ± 13
hGSTA2/F110V	85 ± 50	5.4 ± 3.7	71 ± 42	13 ± 1**
hGSTA2/S215A	21 ± 1	0.3 ± 0.04	17 ± 1	57 ± 5**
hGSTA2/SIFS[b]	9 ± 0.4**	0.2 ± 0.04*	8 ± 0.3**	40 ± 4

[a] GST activity was determined as a function of varying CDNB concentrations (0.1−1.2 mM) at a fixed concentration of GSH (1 mM) at 25 °C. Kinetic parameters were estimated by fitting a hyperbolic function to the experimental data points through nonlinear regression analysis, and are shown ± asymptotic standard error. Except for the K_m ($p > 0.25$), other kinetic parameters between the wild-type hGSTA1-1 and wild-type hGSTA2-2 were statistically significantly different ($p < 0.001$). The statistical significance between a given mutant and the wild-type hGSTA2-2 is denoted as follows: *$p < 0.1$; **$p \leq 0.02$. [b] hGSTA2-2 variant with combined mutations of S9F, I11A, F110V, and S215A.

tively, in comparison with those of the wild-type hGSTA2-2, leading to an approximate 1.5-fold increase in catalytic efficiency of the mutant protein (Table 1). On the other hand, the S215A mutation caused a pronounced decrease in catalytic efficiency of the protein (0.06 $mM^{-1}\,s^{-1}$) due to an approximate 61% reduction in the V_{max} and about 1.5-fold increase in the K_m of the mutant protein (Table 1). The enantioselectivity of hGSTA2-2 was not significantly altered upon F110V mutation (Figure 4b) or S9F or S215A mutation (data not shown). We also generated a quadruple mutant of hGSTA2-2 to mimic the H-site of hGSTA1-1 by mutating S9F, I11A, F110V, and S215A together (hGSTA2/SIFS). Interestingly, the hGSTA2/SIFS mutant was a more efficient catalyst of (+)-*anti*-BPDE−GSH conjugation than either wild-type hGSTA1-1 or wild-type hGSTA2-2 (Table 1). Similar to the wild-type hGSTA1-1, the hGSTA2-2/SIFS mutant protein exhibited a preference toward GSH conjugation of the (+)-*anti*-BPDE enantiomer (Figure 4c).

Kinetic Constants for the Wild-Type and the Mutant Enzymes toward (−)-anti-BPDE. Table 3 summarizes the kinetic constants for the wild-type and the mutant enzymes for GSH conjugation of (−)-*anti*-BPDE. Similar to the (+)-*anti*-BPDE isomer, the wild-type hGSTA1-1 isozyme was a relatively more efficient catalyst of (−)-*anti*-BPDE−GSH conjugation compared with the wild-type hGSTA2-2. The catalytic efficiency of hGSTA2-2 was statistically significantly reduced upon I11A and S215A mutations. Interestingly, the F110V mutation caused an approximate 1.7-fold increase in the catalytic efficiency of the enzyme toward (−)-*anti*-BPDE. Similar to the (+)-*anti*-BPDE isomer, the hGSTA2/SIFS mutant exhibited the highest catalytic efficiency for (−)-*anti*-BPDE−GSH conjugation (Table 3).

Kinetic Constants for the Wild-Type and the Mutant Enzymes toward CDNB. The kinetic constants for the wild-type and the mutant enzymes toward model GST substrate CDNB were also determined, and the data are summarized in Table 4. The catalytic efficiency of the wild-type hGSTA1-1 toward CDNB was approximately 5.1-fold higher compared with that of the wild-type hGSTA2-2. Interestingly, the catalytic efficiency of hGSTA2-2 toward CDNB was moderately increased upon I11A (about 43% higher) and S215A (about 90% higher) mutations. However, the catalytic efficiency of the hGSTA2/SIFS mutant, which exhibited the highest efficiency toward both isomers of *anti*-BPDE, was only slightly different from that of the wild-type hGSTA2-2. The catalytic efficiency of the hGSTA2/F110V mutant was about 57% lower compared with that of the wild-type hGSTA2-2 (Table 4).

Structural Interpretation of the Kinetic Data. Recently, we solved the crystal structures of murine GSTA1-1 in complex with GSH conjugate of (+)-*anti*-BPDE (GSBpd) (*45*), mGSTA2-2·GSBpd complex (*46*), and the two naturally occurring allelic variants of hGSTP1-1 in complex with GSBpd (*47*). However, only two distinct binding modes of

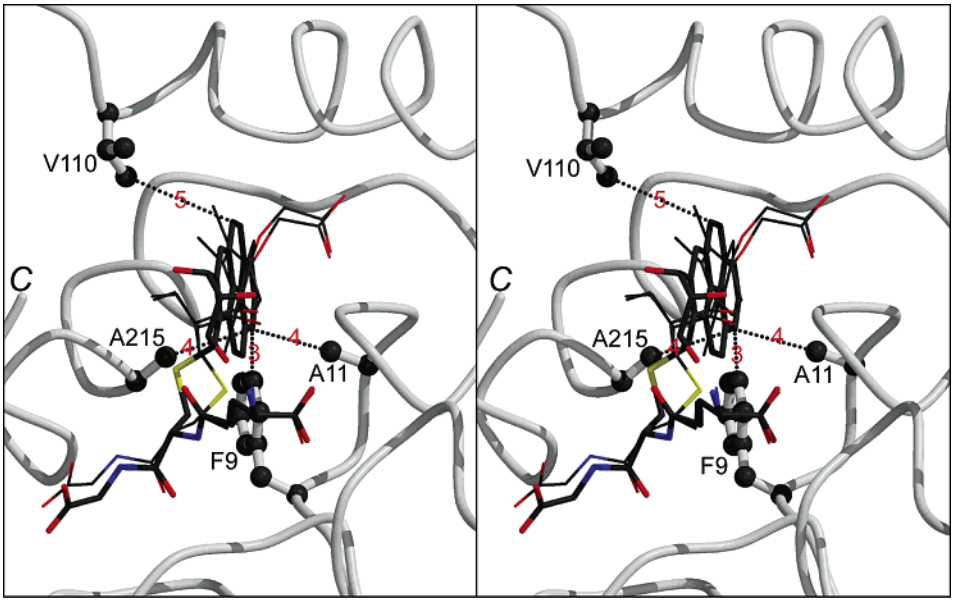

FIGURE 5: Stereoview showing the active center of hGSTA1 in complex with GSEa, the GSH conjugate of ethacrynic acid (*48*). The Cα trace of protein is illustrated as gray pipes, the side chains of F9, A11, V110, and A215 are illustrated as ball-and-stick models in atomic color scheme (carbon in black, nitrogen in blue, oxygen in red, and sulfur in yellow), and GSEa (two conformations) is illustrated as thinner stick models. Also shown is GSBpd, the GSH conjugate of (+)-*anti*-BPDE in the conformations of binding mode 1 (see the text for details), as a thicker stick model, which is adjusted and superimposed with GSEa. The closest distances (Å, in red) between the four sides chains and the BPDE moiety are indicated with dotted lines. This figure was generated with MOLSCRIPT (*51*) and RASTER3D (*52*).

GSBpd were observed in the four structures, one in mGSTA2-2 and hGSTP1-1[I104,A113] (binding mode 1) and the other in mGSTA1-1 and hGSTP1-1[V104,A113] (binding mode 2) (see Figure 2c in ref *46* for the alignment of the four structures). We also found that binding mode 1 of GSBpd is associated with lower catalytic activity most likely because the GSH sulfur is beyond the hydrogen bond distance of the hydroxyl group of GST's catalytic tyrosine residue (*46*). In the present study, we have docked the GSBpd molecule into the active site of hGSTA1-1 in complex with the GSH conjugate of ethacrynic acid (GSEa) (*48*). However, we can do so only when the GSBpd molecule assumes the conformation of binding mode 1 (Figure 5), suggesting that hGSTA1-1 should have a generally low catalytic activity toward (+)-*anti*-BPDE. Nevertheless, the catalytic activity of hGSTA1-1 is >5-fold higher than that of hGSTA2-2 (Table 1). The H-site residues of the two isozymes differ in four positions, including residues 9, 11, 110, and 215. In hGSTA1-1, the four residues are F9, A11, V110, and A215, whereas the corresponding residues in hGSTA2-2 are S9, I11, F110, and S215, among which residue 9 is smaller than that in hGSTA1-1 but the rest become bulkier. As illustrated in Figure 5, F9, A11, V110, and A215 of hGSTA1-1 provide favorable hydrophobic interactions with the BPDE moiety. Therefore, the bulkier side chains of I11, F110, and S215 will impose unfavorable steric interactions with the BPDE moiety; although S9 of hGSTA2-2 is smaller than F9 of hGSTA1-1, I11 and S215 prevent the BPDE moiety from moving toward S9 (not shown). Consequently, hGSTA2-2 should exhibit an even lower catalytic activity toward (+)-*anti*-BPDE, which is consistent with the kinetic data of the hGSTA2-2 variant with combined mutations of S9F, I11A, F110V, and S215A (Table 3). Among residues 11, 110, and 215, residue 11 appears to have the biggest impact on the catalytic activity of the enzyme toward (+)-*anti*-BPDE (Table 1), which is readily explainable when the mobility of these three residues in the structure is taken into account. The mobility of a residue, suggested by its *B* factor, is correlated with the rigidity of the structural motif in which it is located. In the crystal structure of hGSTA1-1 in complex with GSEa, the *B* factors of the Cα atoms of residues 11, 110, and 215 are 19.6, 48.3, and 47.6 Å, respectively (*48*). A similar trend of the *B* factors of these three residues is also observed in other crystal structures of hGSTA1-1. Therefore, residue 11 is located in a more rigid structural motif, and the A11I mutation should have a much more profound steric impact on the BPDE moiety than the V110F and A215S mutations. Our kinetic data of single mutants have demonstrated that this is indeed the case (Table 1). Structural interpretation of the kinetic data toward (−)-*anti*-BPDE is not possible in the absence of the actual three-dimensional structure of hGSTA1-1 or hGSTA2-2 in complex with GSH conjugate of (−)-*anti*-BPDE.

Table 5: Catalytic Efficiencies of Different Classes of Human GST Isozymes and Murine Class α GSTs toward (+)-*anti*-BPDE

isozyme	k_{cat}/K_m (mM^{-1} s^{-1})	ref	isozyme	k_{cat}/K_m (mM^{-1} s^{-1})	ref
Human GST Isozymes					
hGSTA1-1	1.1	present study	hGSTM1-1	10.5	12
hGSTA2-2	0.2	present study	hGSTP1-1	3.7	12
Murine GST Isozymes					
mGSTA1-1	131	*50*	mGSTA3-3	1.7	43
mGSTA2-2	40	*50*	mGSTA4-4	0.2	43

Biological Relevance of hGSTA1-1-Catalyzed GSH Conjugation of anti-BPDE. The catalytic efficiency of hGSTA1-1 or hGSTA2-2 for GSH conjugation of (+)-*anti*-BPDE is considerably lower compared with that of the μ (hGSTM1-1) or π (hGSTP1-1) class human GST isozymes (Table 5; *10*−*12*, *49*). Despite a lower activity, however, hGSTA1-1 is likely to play a major role in protection against carcinogenic effects of *anti*-BPDE in human liver, which is the major site of xenobiotic transformation, because the expres-

sion of hGSTP1-1 is very low in adult human liver and hGSTM1-1 is absent in about 50% of Caucasians due to gene deletion (*21*, *22*). hGSTA1-1 may also play an important role in detoxification of (+)-*anti*-BPDE in human lung, which is a target organ for BP-induced carcinogenesis, due to its higher abundance (*35*).

As summarized in Table 5, the murine GSTA1-1 is significantly more efficient than the corresponding human GSTA1-1 in catalyzing the GSH conjugation of (+)-*anti*-BPDE (ref *50* and the present study). The amino acid sequence similarity between murine and human GSTA1-1 is about 75%. The structural basis for such a high disparity in activity of these enzymes toward *anti*-BPDE was poorly understood until recently when we were able to solve the crystal structure of mGSTA1-1 in complex with GSBpd (*45*). These studies revealed that, in comparison with that of mGSTA1-1, the H-site of hGSTA1-1 is narrow due to squeezing of the C-terminal helix (*45*). Consequently, bulky substrates such as (+)-*anti*-BPDE can be more readily accommodated by the H-site of mGSTA1-1 than that of hGSTA1-1.

Conclusions. The results of the present study demonstrate that a single amino acid substitution in position 11 is sufficient to convert hGSTA2-2 to a protein that matches hGSTA1-1 in its catalytic efficiency for GSH conjugation of the potent environmental carcinogen (+)-*anti*-BPDE. The increased catalytic efficiency of hGSTA2/I11A mutant is accompanied by a greater enantioselectivity for the carcinogenic (+)-*anti*-BPDE over (−)-*anti*-BPDE. Further remodeling of the H-site of hGSTA2-2 to mimic that of hGSTA1-1 (S9F, I11A, F110V, and S215A) results in an enzyme whose catalytic efficiency is approximately 13-fold higher than that of the wild-type hGSTA2-2. The increased activity upon mutations can be rationalized by the interactions of the amino acid side chains with the substrate and the orientation of the substrate in the active site, as visualized by molecular modeling.

REFERENCES

1. International Agency for Research on Cancer (1983) *IARC Monographs on the evaluation of the Carcinogenic risk of Chemicals to Humans. Polynuclear Aromatic Compounds, Part 1. Chemical, Environmental, and Experimental Data,* Vol. 32, International Agency for Research on Cancer, Lyon, France.
2. Buening, M. K., Wislocki, P. G., Levin, W., Yagi, H., Thakker, D. R., Akagi, H., Koreeda, M., Jerina, D. M., and Conney, A. H. (1978) Tumorigenicity of the optical enantiomers of the diastereomeric benzo[a]pyrene-7,8-diol-9,10-epoxides in newborn mice: exceptional activity of (+)-7β,8α-dihydroxy-9α,10α-epoxy-7,8,9,-10-tetrahydrobenzo[a]pyrene, *Proc. Natl. Acad. Sci. U.S.A. 75*, 5358−5361.
3. Slaga, T. J., Bracken, W. J., Gleason, G., Levin, W., Yagi, H., Jerina, D. M., and Conney, A. H. (1979) Marked differences in the skin tumor-initiating activities of the optical enantiomers of the diastereomeric benzo(*a*)pyrene 7,8-diol-9,10-epoxides, *Cancer Res. 39*, 67−71.
4. Gelboin, H. V. (1980) Benzo(a)pyrene metabolism, activation and carcinogenesis: role and regulation of mixed-function oxidases and related enzymes, *Physiol. Rev. 60*, 1107−1166.
5. Thakker, D. R., Yagi, H., Levin, W., Wood, A. W., Conney, A. H., and Jerina, D. M. (1985) Polycyclic aromatic hydrocarbons: metabolic activation to ultimate carcinogens, in *Bioactivation of Foreign Compounds* (Anders, M. W., Ed.) pp 177−242, Academic Press, New York.
6. Dipple, A. (1985) in *Polycyclic hydrocarbons and carcinogenesis: an introduction* (Harvey, R. G., Ed.) ACS Symposium Series 283, pp 1−17, American Chemical Society, Washington, DC.
7. Yang, S. K., and Gelboin, H. V. (1976) Nonenzymatic reduction of benzo(a) pyrene diol epoxides to trihydroxypentahydrobenzo-(a)pyrenes by reduced nicotinamide adenine dinucleotide phosphate, *Cancer Res. 36*, 4185−4189.
8. Dock, L., Waern, F., Martinez, M., Grover, P. L., and Jernstrom, B. (1986) Studies on the further activation of benzo[a]pyrene diolepoxides by rat liver microsomes and nuclei, *Chem.-Biol. Interact. 58*, 301−318.
9. Thakker, D. R., Yagi, H., Levin, W., Lu, A. Y. H., Conney, A. H., and Jerina, D. M. (1977) Stereospecificity of microsomal and purified epoxide hydrase from rat liver: hydration of arene oxides of polycyclic hydrocarbons, *J. Biol. Chem. 252*, 6328−6334.
10. Robertson, I. G. C., Guthenberg, C., Mannervik, B., and Jernstrom, B. (1986) Differences in stereoselectivity and catalytic efficiency of three human glutathione transferases in the conjugation of glutathione with 7β,8α-dihydroxy-9α,10α-oxy-7,8,9,10-tetrahydrobenzo(a)pyrene, *Cancer Res. 46*, 2220−2224.
11. Jernström, B., Funk, M., Frank, H., Mannervik, B., and Seidel, A. (1996) Glutathione S-transferase A1-1-catalysed conjugation of bay and fjord region diol epoxides of polycyclic aromatic hydrocarbons with glutathione, *Carcinogenesis 17*, 1491−1498.
12. Sundberg, K., Widersten, M., Seidel, A., Mannervik, B., and Jernström, B. (1997) Glutathione conjugation of bay- and fjord-region diol epoxides of polycyclic aromatic hydrocarbons by glutathione transferases M1-1 and P1-1, *Chem. Res. Toxicol. 10*, 1221−1227.
13. Wood, A. W., Sayer, J. M., Newmark, H. L., Yagi, H., Michaud, D. P., Jerina, D. M., and Conney, A. H. (1982) Mechanism of the inhibition of mutagenicity of a benzo(*a*)pyrene 7,8-diol 9,10-epoxide by riboflavin 5′-phosphate, *Proc. Natl. Acad. Sci. U.S.A. 79*, 5122−5126.
14. Wood, A. W., Huang, M. T., Chang, R. L., Newmark, H. L., Lehr, R. E., Yagi, H., Sayer, J. M., Jerina, D. M., and Conney, A. H. (1982) Inhibition of the mutagenicity of bay-region diol epoxides of polycyclic aromatic hydrocarbons by naturally occurring plant phenols: exceptional activity of ellagic acid, *Proc. Natl. Acad. Sci. U.S.A. 79*, 5513−5517.
15. Sayer, J. M., Yagi, H., Wood, A. W., Conney, A. H., and Jerina, D. M. (1982) Extremely facile reaction between the ultimate carcinogen benzo(*a*)pyrene 7,8-diol 9,10-epoxide and ellagic acid, *J. Am. Chem. Soc. 104*, 5562−5564.
16. Huang, M. T., Wood, A. W., Chang, R. L., Yagi, H., Sayer, J. M., Jerina, D. M., and Conney, A. H. (1986) Inhibitory effect of 3-hydroxy benzo(*a*)pyrene on the mutagenicity and tumorigenicity of (±)-7β,8-dihydroxy-9α,10α-epoxy-7,8,9,10-tetrahydrobenzo-(*a*)pyrene, *Cancer Res. 46*, 558−566.
17. Fields, W. R., Morrow, C. S., Doss, A. J., Sundberg, K., Jernstrom, B., and Townsend, A. J. (1998) Overexpression of stably transfected human glutathione-S-transferase P1-1 protects against DNA damage by benzo[a]pyrene diol-epoxide in human T47D cells, *Mol. Pharmacol. 54*, 298−304.
18. Hu, X., Herzog, C., Zimniak, P., and Singh, S. V. (1999) Differential protection against benzo[a]pyrene-7,8-dihydrodiol-9,-10-epoxide-induced DNA damage in HepG2 cells stably transfected with allelic variants of π class human glutathione S-transferase, *Cancer Res. 59*, 2358−2362.
19. Guo, J., Pan, S. S., and Singh, S. V. (2003) Exceptional activity of murine glutathione transferase A1−1 against (7*R*,8*S*)-dihydroxy-(9*S*,10*R*)-epoxy-7,8,9,10-tetrahydrobenzo[*a*]pyrene-induced DNA damage in stably transfected cells, *Mol. Carcinog. 36*, 67−73.
20. Srivastava, S. K., Xia, H., Pal, A., Hu, X., Guo, J., and Singh, S. V. (2000) Potentiation of benzo[a]pyrene-induced pulmonary and forestomach tumorigenesis in mice by D,L-buthionine-S,R-sulfoximine-mediated tissue glutathione depletion, *Cancer Lett. 153*, 35−39.
21. Mannervik, B. (1985) The isoenzymes of glutathione transferase, *Adv. Enzymol. Relat. Areas Mol. Biol. 57*, 357−417.
22. Hayes, J. D., and Pulford, D. J. (1995) The glutathione S-transferase supergene family: regulation of GST* and the contribution of the isoenzymes to cancer chemoprotection and drug resistance, *Crit. Rev. Biochem. Mol. Biol. 30*, 445−600.
23. Mannervik, B., Alin, P., Guthenberg, C., Jensson, H., Tahir, M. K., Warholm, M., and Jornvall, H. (1985) Identification of three classes of cytosolic glutathione transferase common to several mammalian species: correlation between structural data and enzymatic properties, *Proc. Natl. Acad. Sci. U.S.A. 82*, 7202−7206.

24. Meyer, D. J., Coles, B., Pemble, S. E., Gilmore, K. S., Fraser, G. M., and Ketterer, B. (1991) Theta, a new class of glutathione transferases purified from rat and man, *Biochem. J. 274*, 409−414.
25. Harris, J., Coles, B., Meyer, D. J., and Ketterer, B. (1991) The isolation and characterization of the major glutathione *S*-transferase from the squid *Loligo valgaris*, *Comp. Biochem. Physiol. 98B*, 511−515.
26. Pemble, S. E., Wardle, A. F., and Taylor, J. B. (1996) Glutathione *S*-transferase class kappa: characterization by cloning of mitochondrial GST and identification of a human homologue, *Biochem. J. 319*, 749−754.
27. Board, P. G., Baker, R. T., Chelvanayagam, G., and Jermiin, L. S. (1997) Zeta, a novel class of glutathione transferases in a range of species from plants to humans, *Biochem. J. 328*, 929−935.
28. Tu, C. P. D., and Qian, B. (1986) Human liver glutathione *S*-transferases: complete primary sequence of an H_a subunit cDNA, *Biochem. Biophys. Res. Commun. 141*, 229−237.
29. Rhoads, D. M., Zarlengo, R. P., and Tu, C. P. D. (1987) The basic glutathione S-transferases from human livers are products of separate genes, *Biochem. Biophys. Res. Commun. 145*, 474−481.
30. Johansson, A., and Mannervik, B. (2001) Human glutathione transferase A3-3, a highly efficient catalyst of double-bond isomerization in the biosynthetic pathway of steroid hormones, *J. Biol. Chem. 276*, 33061−33065.
31. Board, P. G. (1998) Identification of cDNAs encoding two human alpha class glutathione transferases (GSTA3 and GSTA4) and the heterologous expression of GSTA4-4, *Biochem. J. 330*, 827−831.
32. Hubatsch, I., Ridderstrom, M., and Mannervik, B. (1998) Human glutathione transferase A4-4: an alpha class enzyme with high catalytic efficiency in the conjugation of 4-hydroxynonenal and other genotoxic products of lipid peroxidation, *Biochem. J. 330*, 175−179.
33. Zhao, T. J., Singhal, S. S., Piper, J. T., Cheng, J. Z., Pandya, U., Clark-Wronski, J., Awasthi, S., and Awasthi, Y. C. (1999) The role of human glutathione S-transferases hGSTA1-1 and hGSTA2-2 in protection against oxidative stress, *Arch. Biochem. Biophys. 367*, 216−224.
34. Rowe, J. D., Nieves, E., and Listowsky, I. (1997) Subunit diversity and tissue distribution of human glutathione S-transferases: interpretations based on electrospray ionization-MS and peptide sequence-specific antisera, *Biochem. J. 325*, 481−486.
35. Singhal, S. S., Saxena, M., Ahmad, H., Awasthi, S., Haque, A., and Awasthi, Y. C. (1992) Glutathione S-transferase of human lung: characterization and evaluation of the protective role of the alpha-class isozymes against lipid peroxidation, *Arch. Biochem. Biophys. 299*, 232−241.
36. Dreij, K., Sundberg, K., Johansson, A., Nordling, E., Seidel, A., Persson, B., Mannervik, B., and Jernström, B. (2002) Catalytic activities of human alpha class glutathione transferases towards carcinogenic dibenzo[a,1]pyrene diol epoxides, *Chem. Res. Toxicol. 15*, 825−831.
37. Sinning, I., Kleywegt, G. J., Cowan, S. W., Reinemer, P., Dirr, H. W., Huber, R., Gilliland, G. L., Armstrong, R. N., Ji, X., Board, P. G., Olin, B., Mannervik, B., and Jones, T. A. (1993) Structure determination and refinement of human alpha class glutathione transferase A1-1, and a comparison with the Mu and Pi class enzymes, *J. Mol. Biol. 232*, 192−212.
38. Simons, P. C., and Vander Jagt, D. L. (1977) Purification of glutathione S-transferases from human liver by glutathione-affinity chromatography, *Anal. Biochem. 82*, 334−341.
39. Singh, S. V., Leal, T., Ansari, G. A. S., and Awasthi, Y. C. (1987) Purification and characterization of glutathione S-transferases of human kidney, *Biochem. J. 246*, 179−186.
40. Habig, W. H., Pabst, M. J., and Jakoby, W. B. (1974) Glutathione S-transferases: the first enzymatic step in mercapturic acid formation, *J. Biol. Chem. 249*, 7130−7139.
41. Bradford, M. M. (1976) A rapid and sensitive method for the quantitation of microgram quantities of protein utilizing the principle of protein-dye binding, *Anal. Biochem. 72*, 248−254.
42. Laemmli, U. K. (1970) Cleavage of structural proteins during the assembly of the head of bacteriophage T4, *Nature 227*, 680−685.
43. Hu, X., Srivastava, S. K., Xia, H., Awasthi, Y. C., and Singh, S. V. (1996) An alpha class mouse glutathione S-transferase with exceptional catalytic efficiency in the conjugation of glutathione with 7β,8α-dihydroxy-9α,10α-oxy-7,8,9,10-tetrahydrobenzo(a)-pyrene, *J. Biol. Chem. 271*, 32684−32688.
44. Pal, A., Gu, Y., Herzog, C., Srivastava, S. K., Zimniak, P., Ji, X., and Singh, S. V. (2001) Role of arginine-216 in catalytic activity of murine alpha class glutathione transferases mGSTA1-1 and mGSTA2-2 towards carcinogenic diol epoxides of polycyclic aromatic hydrocarbons, *Carcinogenesis 22*, 1301−1305.
45. Gu, Y., Singh, S. V., and Ji, X. (2000) Residue R216 and catalytic efficiency of a murine class alpha glutathione *S*-transferase towards benzo[*a*]pyrene 7(*R*),8(*S*)-diol 9(*S*),10(*R*)-epoxide, *Biochemistry 39*, 12552−12557.
46. Gu, Y., Xiao, B., Wargo, H. L., Bucher, M. H., Singh, S. V., and Ji, X. (2003) Residues 207, 216, and 221 and the catalytic activity of mGSTA1−1 and mGSTA2-2 towards benzo[*a*]pyrene-(7*R*,8*S*)-diol-(9*S*,10*R*)-epoxide, *Biochemistry 42*, 917−921.
47. Ji, X., Blaszczyk, J., Xiao, B., O'Donnell, R., Hu, X., Herzog, C., Singh, S. V., and Zimniak, P. (1999) Structure and function of residue 104 and water molecules in the xenobiotic substrate-binding site in human glutathione S-transferase P1-1, *Biochemistry 38*, 10231−10238.
48. Cameron, A. D., Sinning, I., L'Hermite, G., Olin, B., Board, P. G., Mannervik, B., and Jones, T. (1995) Structural analysis of human alpha-class glutathione transferase A1-1 in the apo-form and in complexes with ethacrynic acid and its glutathione conjugate, *Structure 3*, 717−727.
49. Hu, X., Xia, H., Srivastava, S. K., Herzog, C., Awasthi, Y. C., Ji, X., Zimniak, P., and Singh, S. V. (1997) Activity of four allelic forms of glutathione S-transferase hGSTP1-1 for diol epoxides of polycyclic aromatic hydrocarbons, *Biochem. Biophys. Res. Commun. 238*, 397−402.
50. Xia, H., Pan, S., Hu, X., Srivastava, S. K., Pal, A., and Singh, S. V. (1998) Cloning, expression, and biochemical characterization of a functionally novel alpha class glutathione S-transferase with exceptional activity in the glutathione conjugation of (+)-*anti*-7,8,-dihydroxy-9,10-oxy-7,8,9,10-tetrahydrobenzo(a)pyrene, *Arch. Biochem. Biophys. 353*, 337−348.
51. Kraulis, P. J. (1991) MOLSCRIPT: a program to produce both detailed and schematic plots of protein structures, *J. Appl. Crystallogr. 24*, 946−950.
52. Merritt, E. A., and Bacon, D. J. (1997) RASTER3D: photorealistic molecular graphics, *Methods Enzymol. 277*, 505−524.

BI049435F